Experimental Investigation of Magnetic Field Dependence of Supercurrent in Multiply Connected Superconducting Films*

Anil K. Bhatnagar
Department of Physics, St. John's University, Jamaica, New York 11432

Edward A. Stern
Department of Physics, University of Washington, Seattle, Washington 98195

(Received 19 September 1972)

Measurements of supercurrent density in thin films of tin have been made as a function of externally applied magnetic fields. Following the suggestion of Fulde and Ferrell, multiply connected sandwich-type samples of low self-inductance were prepared in order to observe the theoretically predicted gradual decrease of supercurrent due to depairing of superconducting pairs as the magnetic field is increased. Samples of low self-inductance are necessary to modify the normally observed first-order superconducting transition to a second-order one. Using samples of a suitable geometry, we have observed both total disappearance of supercurrent due to complete electron depairing in tin films and also the change from first to second order of the superconducting transition induced by an external magnetic field. Various experimental checks were made to verify that the decrease in supercurrent with increasing magnetic field was due to depairing and not spurious effects. The data have been analyzed to deduce supercurrent density versus the vector potential, the critical vector potential at which complete depairing takes place, the maximum current density, and their temperature dependences. The quantitative agreement between the experimental results and the predictions of the Ginzburg–Landau theory and its microscopic extensions is reasonably good.

I. INTRODUCTION

Current-induced transitions[1] in thin superconducting films have been extensively studied for a long time by two experimental methods: (i) A film is used as a circuit element in series with a current source; (ii) a supercurrent is induced in a multiply connected film placed in an axially variable magnetic field. Both of these methods have shown that the transition from superconducting to normal state takes place discontinuously when a critical current density is reached. On the theoretical side the current carrying state of a superconductor has been a subject of extensive investigation. Rogers,[2] Bardeen,[3] Paramenter,[4] Fulde and Ferrell,[5] and Maki[6] have discussed in detail the dependence of the current on the total momentum of the Cooper pairs.[7,8] The theoretical prediction is that the current initially increases linearly with increased momentum, reaches a maximum, and then starts decreasing gradually as the total pairing momentum increases beyond the value at which Cooper pairs begin to become unstable with respect to the break up into quasiparticle excitations. The current finally vanishes at a critical value of the total pairing momentum. Thus the theory predicts that the current-induced depairing should provide a gradual decrease in the order parameter and finally a second-order phase transition. There are other experimental methods to produce depairing which are theoretically analogous[9] to dc current flow. These experiments[10] have shown the predicted depairing behavior. However, until the completion of the experiments[11] reported here, none of the experimental investigations had confirmed the depairing behavior in dc current flow. In all cases a transition of the first order was observed instead of the predicted second order.

The discrepancy between the theory and the experiments has been discussed by Fulde and Ferrell[5] who showed that the normally observed first-order transition is not a true indication of the basic nature of the coherence in a superconducting state; it is a result of the particular experimental arrangement. An abrupt loss of superconducting coherence in the first experimental arrangement takes place in which a film is used as a circuit element because the critical conditions are reached when the supercurrent density (controlled by an external source) attains its maximum value. If more than this maximum current is forced through the film, the film must transform to its normal state and we obtain a first-order transition since we change from a state of finite order parameter to one of zero. The second experimental arrangement in which a multiply connected film is placed in a variable magnetic field is a more suitable arrangement since the velocity of the electron pairs (therefore the total pairing momentum) is determined by the inductive coupling with the variable magnetic field and therefore it can adjust itself freely. The failure to observe the depairing behavior in these experimental arrangements was attributed to a large value of self-inductance of the

investigated samples which perturbs the vector potential produced by the external field and influences the nature of the superconducting transition. It was suggested[5] that one might hope to verify the depairing behavior by investigating samples having extremely small self-inductance. We have previously reported the successful observation of depairing behavior induced to by dc current flow in samples prepared so as to have small self-inductance.[11–13] Recently, Hansen[14] also reported an observation of a decrease in supercurrent in multiply connected indium films after reaching its maximal value as a function of external magnetic field using a different technique. However, owing to some experimental difficulties he was not able to observe a second-order superconducting transition which we have successfully observed and reported previously.[11–13] Groff and Parks[15] have also recently interpreted their results on fluxoid-quantization experiments on cylindrical aluminum films to obtain the temperature dependence of the critical pairing momentum (at which total depairing takes place) in a limited temperature range near the transition temperature.

Subsequent to these experiments, the feasibility of observing the depairing regime all of the way to the second-order transition was questioned by Schmid[16] and Hansen and Christiansen,[17] who argued that fluctuations would make the region past the maximum current unstable. In Sec. V we discuss our criticisms of these fluctuation calculations and give experimental evidence to prove that our measurements are not spurious.

This paper discusses details of the experimental investigation of the supercurrent in thin tin films as a function of the vector potential in the film as reported earlier.[11–13] A detailed comparison of the experimental results with the Ginzburg–Landau theory[18] and its microscopic extensions is presented. Theoretical background for the motivation of the experiment is developed in Sec. II. Section III describes the experimental details. The experimental results and the analysis of the data is presented in Sec. IV, and Sec. V discusses the results and is followed by the conclusions.

II. THEORETICAL CONSIDERATIONS

A relation between the supercurrent density J_s in a superconductor and the total pairing momentum $2q$ of the Cooper pairs can be easily obtained using the Ginzburg–Landau theory and is given by

$$J_s = eN_s(q/m)(1 - q^2/q_c^2) , \tag{1}$$

where e and m are the electronic charge and mass, respectively; N_s is the number of superconducting electron pairs in absence of a current, and q_c is that value of q at which J_s vanishes owing to complete depairing of electron pairs in the superconductor. In deriving Eq. (1) the order parameter and the supercurrent density are assumed to be spatially independent; this constraint requires that

$$\tau < \xi(T) , \quad \lambda(T) , \tag{2}$$

where τ is the thickness of superconductor and $\xi(T)$ is the temperature-dependent coherence length. J_s is plotted as a function of q in Fig. 1. The interesting feature of Eq. (1) is that J_s reaches a maximum value J_{sm} at $q = q_m = q_c/3^{1/2}$ and then decreases monotonically to zero at $q = q_c$. This decrease in the supercurrent is due to current-induced depairing of electron pairs into individual quasiparticle excitations, thus reducing the number N_s. Similar features of a q dependence of J_s are also obtained in other theories[2–6] as well. The most important aspect of this gradual decrease of supercurrent is that it provides a gradual decrease in the order parameter and finally a second-order superconducting transition to the normal state at $q = q_c$. The important feature of Eq. (1), that J_s should decrease for $q > q_m$, was not verified directly or indirectly by various experiments reported previously. Tunneling measurements by Mitescu[19] and by Levine[20] performed on superconducting films barely reached the region where $q \simeq q_m$. In this region the energy gap was found to be somewhat depressed by the transport current through the film as expected theoretically. Critical-current measurement by Mercereau and Crane,[21] and microwave-transmission measurements by Rose and Sherrill[22] also failed to show any depairing behavior for $q > q_m$.

The most suitable geometry for a superconducting sample to permit the observance of the magnetic-field-induced depairing in the film is a multiply connected geometry as suggested by Fulde and Ferrell.[5] To explain why Mercereau and Crane[21] observed a first-order superconducting transition in their hollow-cylinder superconducting films, and the importance of a suitable geometry for the sample, consider a multiply connected superconducting film with its axis parallel to an external variable magnetic field. If the film thickness τ is thin compared to $\lambda(T)$ and $\xi(T)$, then the following London-type equation relates the current per unit length J which flows around the axis of the film and the vector potential A seen by J:

$$J = -(c\tau/4\pi\lambda^2)A_c F(A/A_c) , \tag{3}$$

where A_c is the critical vector potential and is proportional to q_c, c is the velocity of light, $F(A/A_c)$ is a function of (A/A_c) which is equal to (A/A_c) for $(A/A_c) \ll 1$ and goes to zero smoothly at $(A/A_c) = 1$. It is further assumed that the film has trapped no flux. In the Ginzburg–Landau theory one can write

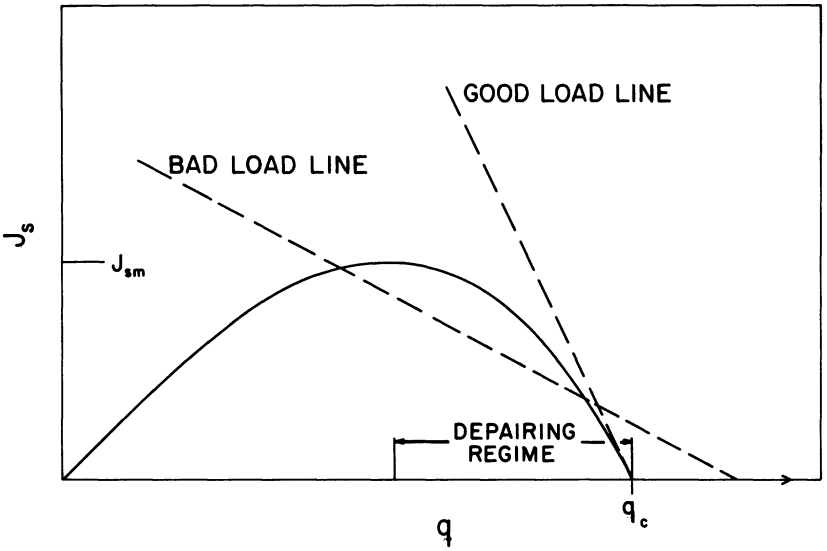

FIG. 1. Dependence of supercurrent density J_s on pairing momentum q (vector potential A) along with two load lines. q_c (A_c) refers to the critical pairing momentum (vector potential) at which J_s reduces to zero owing to complete current-induced depairing.

$$F(A/A_c) \propto (A/A_c)(1 - A^2/A_c^2) \tag{4}$$

and

$$\vec{A} = (c/e)\vec{q}\,, \tag{4a}$$

when the local theory is applicable. In other theories similar features are retained for $(A/A_c) \ll 1$ and $(A/A_c) = 1$.

In making a comparison between the experimental results and Eq. (1) it is usually assumed that the vector potential A is entirely due to the external magnetic field H_{ex} which induces the current J in the film. This is, however, not correct since the induced-current J sets up its own magnetic field which adds to the vector potential A_{ex} due to H_{ex}. Thus experimentally the vector potential A which enters in Eq. (3) is not A_{ex} but is given by

$$A = A_{ex} - A_s\,, \tag{5}$$

where A_s is due to the field self-induced by J, and the following relations hold:

$$\oint \vec{A}_{ex} \cdot d\vec{l} = \int\int \vec{H}_{ex} \cdot d\vec{s} = \phi_{ex}\,, \tag{6}$$

$$\oint \vec{A}_s \cdot d\vec{l} = -\oint (L/l)\vec{J} \cdot d\vec{l} = LJ = \phi_s\,, \tag{7}$$

where L is the self-inductance of a unit length of the sample, l is the current path length, $\oint dl = l$, $\int\int ds = S$ is the area enclosed by the film, ϕ_{ex} and ϕ_s are the fluxes corresponding to A_{ex} and A_s, respectively. Because of the diamagnetic property of superconductors the self-induced A_s is opposite in sign to A_{ex}. The experimental complications arise because of Eq. (5) since one cannot apply A to the sample directly but instead applies A_{ex}. The value of A that one obtains is determined by the simultaneous solutions of Eqs. (3) and (5). This can be done graphically for a fixed A_{ex} by plotting J as given by both Eqs. (3) and (5) as shown in Fig. (1). The intersection of the two curves then determines both A and J. The relation (5) is analogous to a linear load line in electrical circuit theory. In Eq. (3) for the value of A where depairing becomes a large effect, J decreases with increasing A. The depairing region in the J-vs-A curve is analogous to a negative resistance region in electrical circuit theory and this region can be measured only if the slope of the load line is equal or greater than the slope of the depairing curve, so that there is only one intersection of curves given by Eqs. (3) and (5). When this condition is satisfied the load line is referred to as a good load line. However, if there are two intersections as would be the case for a small sloped load line, which is referred to as a bad load line, then only the intersection corresponding to the smaller value of A would be experimentally accessible. As A_{ex} is increased for a bad load line, a maximum value of A is reached for which J is still finite and beyond which there are no further intersections. At this point the sample switches discontinuously along the load line to the $J = 0$ state, that is, the normal state, the usually observed first-order transition. In a good load line situation, only one intersection of curves (3) and (5) is obtained and therefore experimentally the complete curve of Eq. (3), as shown in Fig. 1, is accessible and a second-order transition to $J = 0$ should be observable.

It is of interest then to find a criterion for a good load line condition in terms of sample parameters which can be controlled. In the experiments reported here the measured quantity is flux rather than the vector potential A or the current J; therefore Eqs. (3) and (5) should be rewritten in terms of the flux associated with A_{ex}, A_s, and J using relations (6) and (7). These are

$$\frac{\phi_s}{\phi_c} = \frac{\tau S}{\lambda^2 l} F\left(\frac{\phi}{\phi_c}\right) = \frac{1}{\gamma} F\left(\frac{\phi}{\phi_c}\right) , \tag{8}$$

$$\phi_s = \phi_{ex} - \phi , \tag{9}$$

where $\gamma = \lambda^2 l/\tau S$ and

$$\phi_c = \oint \vec{A}_c \cdot d\vec{l} . \tag{10}$$

Equations (8) and (9) can be combined to yield

$$F\left(\frac{\phi}{\phi_c}\right) = -\frac{\lambda^2 l}{\tau S}\left(\frac{\phi}{\phi_c} - \frac{\phi_{ex}}{\phi_c}\right) . \tag{11}$$

The right-hand side of Eq. (11) when plotted as a function of ϕ/ϕ_c represents a straight line with a slope of $(-\lambda^2 l/\tau S)$, and the intersection of this line with the curve $F(\phi/\phi_c)$ gives the solution of Eq. (11). The maximum magnitude of the slope of $F(\phi/\phi_c)$ is -2 occurring at $\phi = \phi_c$ in simple Ginzburg–Landau (GL) theory. Thus the required condition for a good load line is

$$\gamma \equiv \frac{\lambda^2 l}{\tau S} \geq |\text{maximum slope of } F(\phi/\phi_c)| \tag{12}$$

or $\gamma \geq 2$ in the GL theory. For a cylindrical film of thickness τ and radius R this condition reduces to

$$2\lambda^2/\tau R \geq 2 . \tag{13}$$

This has previously been shown by Douglass.[23] Assuming $\lambda = 10^{-5}$ cm and $\tau = 5\times10^{-6}$ cm for a typical sample, R then has to be approximately 5×10^{-5} cm for a good load-line condition. The tin-film sample investigated by Mercereau and Crane[21] had a radius of 5 mm giving a very small value of γ resulting in a bad load line situation. Therefore, it is no surprise that a first-order superconducting transition was observed. It is only by making samples which satisfy condition (12) can one hope to completely verify the predicted depairing behavior due to dc current flow in the film.

The requirement that $R = 5\times10^{-5}$ cm for a cylindrical sample is extremely difficult to satisfy experimentally. The situation can be improved, at least theoretically, by making R an order of magnitude larger and the film thickness an order of magnitude smaller. However, this results in other experimental problems because of the very small diamagnetism shown by the sample. One has to look for other multiply connected geometries which satisfy the condition (12) and still be practical for making measurements. Fulde and Ferrell[5] have suggested two geometries which are suitable and can be used to minimize the effect of the self-induced A_s. The first one is a cylindrical film in which the hollow region is partially filled by an inert superconductor leaving only a very small nonsuperconducting area enclosed by the film. The Meissner effect excludes the bulk of the interior region from contributing to the self-inductance L, and therefore to A_s. This geometry has been used successfully by Hansen[14] to observe the decrease of J in the region where $q > q_m$. The second one is a sandwich-type geometry; a thick rectangular film of an inert superconductor on top of which is placed an insulating layer and then on top of this the film to be investigated. In order to have this geometry multiply connected it is essential that the top film makes good electrical contact with the base film at the two edges (lengthwise). By making the insulating layer very thin, the self-inductance of the sample can be reduced to any reasonable desired value. The latter geometry is shown in Fig. 2.

It is interesting to note that γ in the latter two geometries is given by

$$\gamma = \lambda^2/\tau\lambda' , \tag{14}$$

where λ' is equal to the sum of the penetration depth of a magnetic field into the inert superconductor and the thickness of the insulating layer. Comparing (13) and (14) it is seen that R is replaced by $2\lambda'$ in (14). Experimentally, it is much easier to make λ' small enough to realize condition (12). A proper choice of τ and λ' can be made either to have a good load-line condition at all temperatures below the superconducting transition temperature T_c of the film, or to have a bad load-line condition at temperatures far below T_c, which then changes to a good load-line condition near T_c. This is possible because of the temperature dependence of λ, which changes from a constant value λ_0

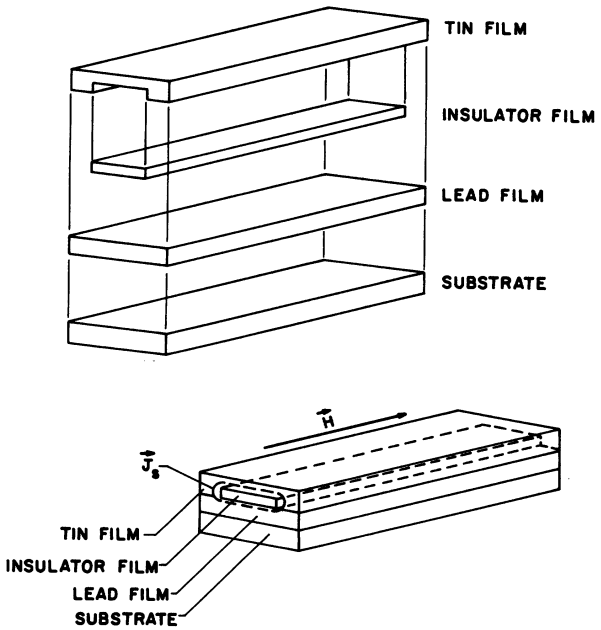

FIG. 2. Exploded view of sandwich-type geometry and the sample. $\vec{J}_s$ shows the path of induced current in presence of magnetic field $\vec{H}$.

at 0 °K to ∞ at T_c. By choosing a sample of the latter characteristics it is possible to observe the change of the superconducting transition from a first- to a second-order one in the same experimental run, and not only verify Eq. (3) but also confirm the importance of the load line in observing the depairing effect.

III. EXPERIMENTAL DETAILS

a. General sample considerations. A multiply connected sample under investigation must satisfy condition (12) to detect the second-order transition. Because of the reasons discussed in Sec. II a plane sample geometry was chosen as illustrated in Fig. 2. This geometry still has the following limitation which must be overcome to assure success in the experiment.

A multiply connected sample in an external magnetic field is similar to a solenoid of finite length in that the induced current density will not be uniform throughout its length, but will be higher at the ends. Consequently, as the magnetic field is increased the ends of the sample will become normal before its central portion and a propagation of a normal region will take place. The true behavior of the film in a magnetic field will be obscured by this undesired effect. This is especially so because the experiments reported here involve the detection of the supercurrent at the two ends of the sample.

In the present work, lead is used for the inert superconductor base, magnesium fluoride for the insulating film, and tin films for the samples under investigation. It is quite easy to obtain a good load-line condition in the sandwich-type geometry, as illustrated in Fig. 2 and discussed in the previous section. Film thicknesses can be accurately determined either by optical methods[24] or a quartz-crystal-oscillator monitor,[25] and edges can be made sharp and distinct if a proper mask is used. To eliminate the end effects an analogy to the concept of guard rings in a condenser[26] is used. This is done by depositing a second film of lead over each end of the tin film leaving the central portion of the tin film uncovered. The lead films make good electrical contact with the tin film. The lead film portions of the sample behave as guard rings to the central portion of the sample. The schematic of the improved geometry of the sample is shown in Fig. 3. Use of the improved geometry makes the current density uniform throughout the exposed length of the tin film. The current density will still be nonuniform and higher at the ends but this does not present any difficulty because of the higher critical field and current for lead. Such samples have been successfully used in the present work.

b. Sample preparation. A pinhole-free gold foil, 10^{-4} in. thick, is used as a substrate to deposit the various films in a high vacuum to make a sample. The gold foil is cut to an approximate size of 1 cm long and 2 mm wide, cleaned with distilled water and dilute nitric acid, and is finally rinsed with clean distilled water and dried. Only a wrinkle-free flat foil is used. The foil is placed flat on a precleaned glass slide and is supported by razor blades with a magnet on the other side of the slide. The glass slide is placed in a vacuum chamber at least 30 cm above the evaporation sources. A large, thick copper plate is placed about 6 in. above the substrate and is cooled to liquid nitrogen temperature to trap condensable gases to obtain a better vacuum. Various masks are attached to a mechanical device which can be rotated manually from outside the vacuum chamber. These masks are used to shadow the substrate to deposit films of the desired geometry.

The sequence of deposition of films is as follows. First a 500-Å film of magnesium fluoride is deposited on the entire surface of the foil to eliminate proximity effects between the gold foil and the superconducting films. The vacuum chamber is brought back to atmospheric pressure and the charges of 99.9999%-pure lead and tin, and magnesium fluoride are placed in their respective evaporating boats. The vacuum system is flushed with dry argon many times to decrease the partial vapor pressure of oxygen in order to minimize oxidation of the sample films. The samples are prepared in a vacuum of 2×10^{-6} torr or better by depositing films of lead (thickness $d_1 \gg \lambda_{Pb}$, the penetration depth of Pb), magnesium fluoride (thickness b), tin (thickness $\tau < \lambda_{Sn}$), and the guard-ring films of lead (thickness $d_2 \gg \lambda_{Pb}$), in this respective order. The film thicknesses are determined by a precalibrated quartz-crystal-oscillator set up. The proper geometries of the films are obtained by using appropriate masks. The sample is prepared with its axis parallel to the long dimension of the gold foil and near one of its ends.

c. Measurement technique. A block diagram of the experimental set up is shown in Fig. 4. The electronics is designed to detect small changes in capacitance of a capacitor, one plate of which is the gold foil with the attached sample. The gold foil is fixed at one end with the other end, where the sample is located, free to vibrate as a cantilever. The amplitude of vibration of the end of the gold foil with the sample is detected by the change in capacitance that it causes. The amplitude of vibration is related to the amount of flux expelled by the sample. This amount of flux expelled is measured as a function of the magnitude of a magnetic field directed along the axis of the superconducting sample and gives the final data which is interpreted in terms of depairing effects.

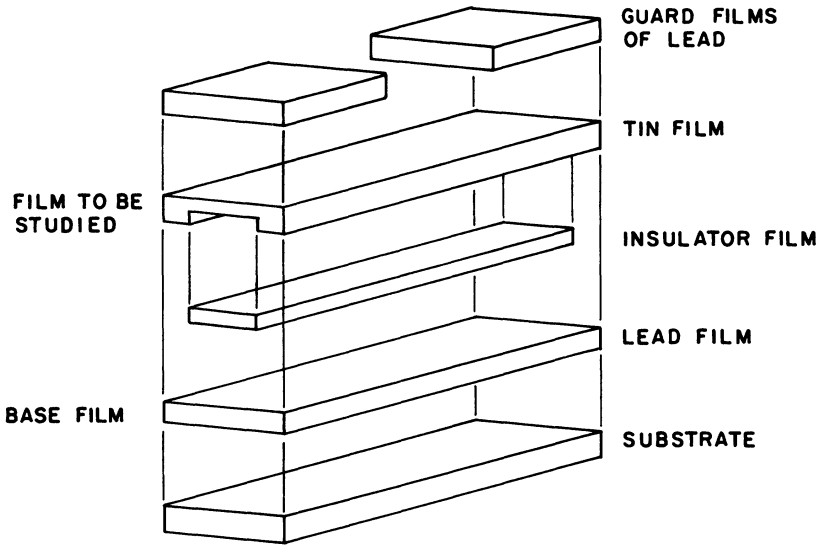

FIG. 3. Exploded view of the improved sandwich-type geometry with lead guard films.

The amount of the expelled flux in the composite sample varies along its length because of the different penetration depths and thickness of the tin and lead films. The magnetic flux is completely expelled from the lead guard-rings portion of the sample because their thicknesses d_1 and d_2 are large compared to λ_{Pb}. The flux is only partially expelled in the tin-film portion of the sample because of the good load-line characteristics of this part of the sample. The distribution of the magnetic flux around the sample in the superconducting state is illustrated in Fig. 5. The change in the expelled flux at the junction of the tin and lead films is directly measured in the experiment by its interaction with a two-dimensional magnetic dipole formed by two parallel wires running perpendicular to the sample axis whose plane is parallel to the sample plane at a distance 0.005–0.010 in. from the sample. An alternating current at the natural resonant frequency of the gold foil cantilever is passed in one direction through one wire of the dipole and in the opposite direction through the other. The wires are spaced apart so that effectively only a few thousandths of an inch on either side of the junction is probed by this dipole driver. The driver produces a net force on the sample only if the induced currents in the sample vary appreciably in the region between the two wires composing the dipole driver, i.e., within a distance of a few thousandths of an inch. In our sample, such a variation occurs only at the junction between the tin and lead guard rings and at the other end of the guard rings at the extreme ends of the sample. By centering the driver wires above the junction we assure that they interact only with the region in the vicinity of the junction. Further

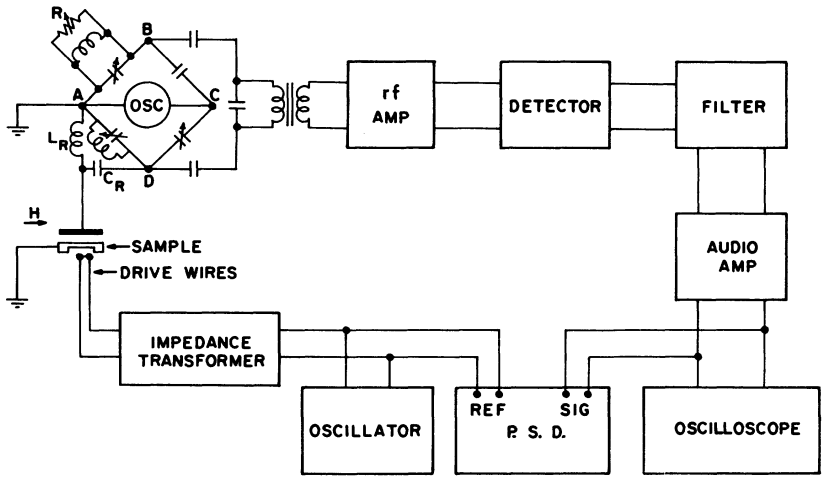

FIG. 4. Block diagram of electronic set up. PSD stands for phase sensitive detector.

details of the dipole driver are given in Ref. 11.

The dipole produces an oscillating force at the superconducting film which is proportional to the difference in the expelled flux at the junction of the lead and tin films. This force in turn produces an amplitude of vibration of the sample directly proportional to the difference of the expelled flux near the junction. The amplitude of vibration is detected by measuring the induced change in capacitance between the moving foil and a fixed reference surface using the experimental arrangement shown in Fig. 4.

d. Sample holder and cryostat. A schematic of the sample holder is shown in Fig. 6. This holder is placed inside a standard double glass Dewar system so that it can be maintained in the liquid-helium temperature range. The gold foil mounted as shown in Fig. 6 forms one plate of capacitor as described above. The fixed reference plate is a $\frac{1}{4}$-in.-diam copper disk soldered to the central conductor of a coaxial line which passes out of the helium-temperature region through a cap (not shown in the figure) which seals the helium-temperature region from the atmosphere. The gold foil is soldered with Cd-Bi solder (which does not become superconducting in the temperature range of interest here) to the flat end of a copper strip which is connected to the outer copper frame using a brass screw. The spacing between the foil and the copper plate is adjusted by moving the upper screw in or out. The copper wires (AWG #32) which act as the magnetic-dipole driver are mounted on a separate copper block.

The full details of the magnetic-dipole-driver holder are given in Ref. 11. As can be seen in Fig. 6, three wires are closely spaced with each other, then a space of approximately 2 mm separates them from another three wires which are again closely spaced. One end of each of the six wires is soldered to a copper block to keep the wires in good thermal contact with the bath to reduce any heating of the sample by a temperature rise in the driver produced by the current in the wires. The other end of the wires is connected to

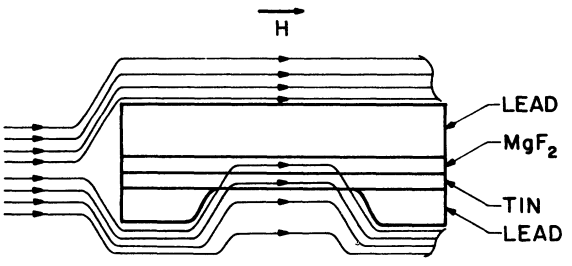

FIG. 5. Distribution of magnetic field inside sample. Sample is shown lengthwise.

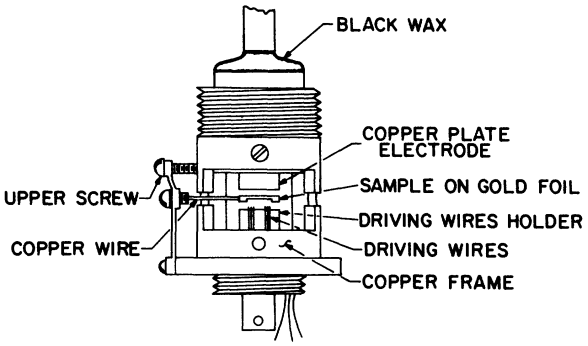

FIG. 6. A schematic of sample holder. See Sec. III *d* for details.

an oscillator through a Kovar seal. Only two wires of the three wires at either end are connected to the oscillator at one time in order to produce a magnetic dipole field at the sample. The pairs of wires chosen is varied to control the desired location of the dipole center and its spacing.

To minimize motion of the gold foil caused by vibrations outside the Dewars, the cryostat, consisting of a double Dewar system, is mounted on shock absorbing materials to attenuate mechanical noise. The noise due to bubbling of liquid nitrogen is reduced by filling the outer Dewar with zeolite.[27] The liquid nitrogen is poured on the zeolite until it just reaches the bottom of the outer Dewar. At this point all of the zeolite is at liquid-nitrogen temperature but no liquid nitrogen remains. The temperature at the bottom of the outer Dewar is monitored by a copper-constantan thermocouple. The inner Dewar, therefore, remains shielded by the zeolite at liquid-nitrogen temperature with *no* liquid to boil and to cause spurious vibrations.

e. Sample and impedance bridge. The gold foil with the sample is cut to an approximate size of 6.5×1.5 mm and is soldered to the sample holder as described in subsection III *d*.

The impedance bridge used to detect the induced changes in capacitance between the fixed reference and the foil is shown in Fig. 4. The bridge is driven with a quartz-crystal oscillator at 46.7 MHz. Further experimental details on the sample mounting and impedance bridge are given in Ref. 11. Suffice it to say that under typical conditions vibrations down to 20-Å peak to peak are detectable.

When the foil vibrates at a frequency ω the bridge's imbalance varies and is detected as a sinusoidal output signal of a 46.7-MHz carrier amplitude modulated by the frequency ω. The amplitude of modulation depends on the relative change of capacitance between the foil and the fixed reference and thus on the amplitude of vibration of the sample. The amplitude-modulated carrier frequency of 46.7 MHz is amplified, rectified, and

filtered. The resulting signal of frequency ω is further amplified by a low noise audio-amplifier and is finally detected using a phase-sensitive detector.

f. Magnetic field. Two square Helmholtz superconducting coils are used to produce the static magnetic field and are mounted on a brass can which encloses the sample holder and can be evacuated. The field is calibrated at room temperature using a magnetometer probe. The earth's magnetic field is cancelled to better than 5 mG in the vicinity of the sample using three mutually perpendicular Helmholtz coils outside the Dewar.

g. Experimental procedure. During a typical run, the vacuum-tight can (with the sample holder inside) is first evacutated, then immersed in liquid helium, and then about 0.1 torr of helium gas is admitted to maintain thermal contact between the sample and the helium bath. The gold-foil cantilever with the sample typically vibrates between 50 and 100 Hz with a "Q" of 50.

Temperatures lower than 4.2 °K are obtained by pumping on the liquid-helium bath and controlling the vapor pressure with the use of a Cartesian manostat. The temperature of the helium bath and therefore of the sample is inferred from the vapor-pressure measurement by a manometer just above the liquid bath. A small heater is placed at the bottom of the inner Dewar to stir the bath and minimize the thermal gradient throughout the liquid helium at temperatures above the λ point. It is estimated that at about 2.5 °K the maximum temperature error is not more than 1% and is less for higher temperatures. Once the desired temperature has been stabilized as monitored by a carbon resistor, the measurement is made.

To measure the transition temperature of the tin film the sample is brought to a temperature of 3 °K and an approximately 20-G field is applied along its axis. The sample is heated locally by a nichrome wire loop for a short time to drive it normal. The sample is allowed to cool again and then the field is switched off. If the sample is multiply connected then it will trap the flux. A small ac current of the same frequency as the natural resonant frequency of the foil cantilever is passed through the magnetic dipole driver to produce an oscillating field at the two junctions of tin and lead films of the sample. The dipole driver's fields are set equal and opposite to each other at each junction, doubling the force driving the sample, and thus doubling the amplitude of vibration for a given trapped flux. If the sample has some trapped flux, the force produced by the driver will have a component at the same frequency as the driver causing the sample to vibrate at this frequency, the amplitude of vibration being proportional to the trapped flux. If there is no trapped flux then the only force between the sample and the driver is that caused by the diamagnetic currents in the sample shielding the driver fields. This force is at twice the driver frequency. We thus can distinguish between the currents induced in the sample by the driver and those produced by an external field. Since the change in temperature from 3 to 4 °K alters the superconducting properties of tin without substantial change in the properties of lead, this procedure is used to determine the transition temperature of tin films. The temperature of the sample is raised continuously from 3 to 4.2 °K and the signal is recorded as a function of temperature. The temperature above which the signal remains constant is taken as the transition temperature. The uncertainty in measurement of the transition temperature of tin films is estimated to be approximately 20 m°K.

The rest of the data were taken by keeping the temperature fixed, varying the static magnetic field and reading the signal on the phase-sensitive-detector output meter. The driving current and other settings are kept unchanged. Before taking data for another temperature the static field is switched off and the sample is heated momentarily to drive it normal in order to expel any trapped flux.

IV. EXPERIMENTAL RESULTS AND THEIR INTERPRETATION

A. Results

Measurements on four samples are reported here. As described in Sec. III, each sample is composed of four different films; a base film of lead, an insulating layer of magnesium fluoride, a tin film, and lead guard films. The thicknesses of these films for each sample are listed in Table I. The experimental data are shown only for samples 3 and 4 in Figs. 7 and 8. The data for sample 1 and 2 are of similar characteristics and are not shown here. Samples 1 and 3 were prepared to satisfy the good load-line condition (12), at least down to 1.5 °K in temperature, while samples 2 and 4 were prepared to show a bad load-line behavior at low temperatures and a good load-line behavior at temperatures close to the transition temperature of the tin film ($T_{c,\mathrm{Sn}}$). This was done intentionally to verify the importance of the load line in making the full current-induced depairing regime experimentally accessible.

The data for sample 3 show that the signal increases linearly with the applied field up to a certain field value, beyond which a departure from the linear behavior is clearly noted. The signal again becomes linear at higher fields. The nonlinear behavior becomes smaller as the temperature is increased towards $T_{c,\mathrm{Sn}}$. At temperatures close to $T_{c,\mathrm{Sn}}$ the signal shows a linear dependence on the

TABLE I. Various parameters of samples and transition temperature of tin films.

Sample	Thickness of base film of lead (Å)	Thickness of insulating layer of MgF_2 (Å)	Thickness of tin film (Å)	Thickness of lead guard films (Å)	Transition temperature of tin film (°K)
1	3102 ± 500	373 ± 95	511 ± 80	1500 ± 500	3.85 ± 0.05
2	3212 ± 65	1792 ± 35	1052 ± 20	2000 ± 40	3.86 ± 0.02
3	3094 ± 60	892 ± 20	411 ± 15	1640 ± 35	3.80 ± 0.02
4	3067 ± 60	2164 ± 40	574 ± 17	1982 ± 40	3.80 ± 0.02

[a]The length and width of the active area of the tin film are approximately 2 and $\frac{3}{4}$ mm, respectively.

applied field in the range of interest. Ordinarily a linear behavior of the signal with the field is expected until the field becomes high enough to drive the film normal, i.e., a catastrophic depairing takes place in the film producing a first-order transition. However, this is certainly not the case here. Similar behavior is observed for sample 4 (sample 2) at all temperatures at which data were taken except at 1.96 °K (2.30 °K for sample 2) at which a sudden increase in the signal is observed at a certain field, beyond which the signal again becomes linear with the field. We show that the gradual nonlinear and sudden increases of the signal are due to second- and first-order transitions, in the superconducting tin film, respectively.

B. Interpretation

To understand the data we refer to Fig. 9(a), which displays a schematic of a cross section through the length of the right half of the sample. At the junction of the lead and tin films there is a discontinuous step in the flux expelled by the sample as described in III c. The observed signal in the experiment is due to the interaction of the driver field with this step in the expelled flux p.

For fixed d_2 in Fig. 9(a) and applied field, the magnitude of p will vary with the temperature of the sample through changes in the supercurrent in the tin film as a result of changes in its $\lambda(T)$. The penetration depth of a magnetic field in lead does not appreciably change below $T_{c,\mathrm{Sn}}$ and therefore the temperature dependence of the signal reflects only the temperature dependence of the supercurrent in the tin film. On the other hand if we keep d_2 and temperature constant, and vary the field, any change in the signal shows the field dependence of the supercurrent in the tin film, if it is assumed that field effects are negligible for lead films. This assumption is valid because the fields used in this experiment are much less than the critical field of bulk lead, $H_{c,\mathrm{Pb}}$.

Figure 10 illustrates how the experimental data is interpreted. If the tin film were not supercon-

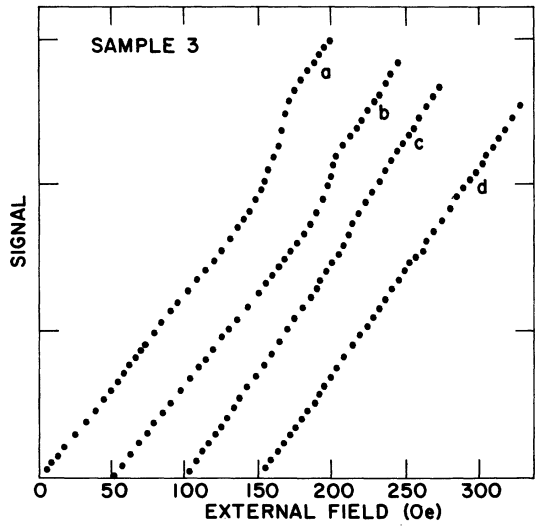

FIG. 7. Measured singal vs magnetic field for sample 3 at (a) 1.78 °K, (b) 2.24 °K, (c) 3.15 °K, and (d) 3.68 °K. Each curve is displaced 50 Oe along the horizontal axis from the previous one. T_c for tin film in this sample is 3.80 °K.

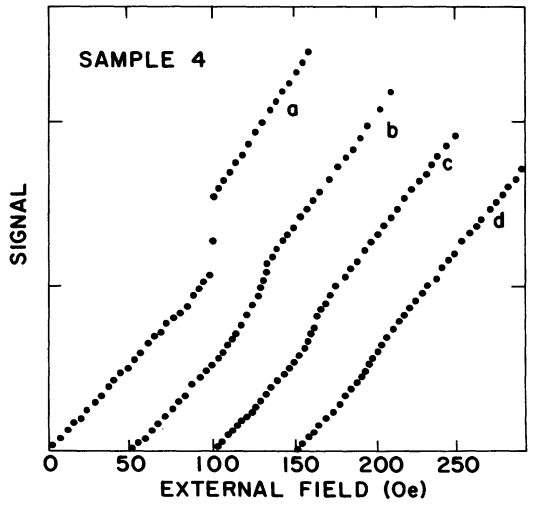

FIG. 8. Measured signal vs magnetic field for sample 4 at (a) 1.96 °K, (b) 2.81 °K, (c) 3.04 °K, and (d) 3.28 °K. Each curve is displaced 50 Oe along the horizontal axis from the previous one. T_c for tin film in this sample is 3.80 °K.

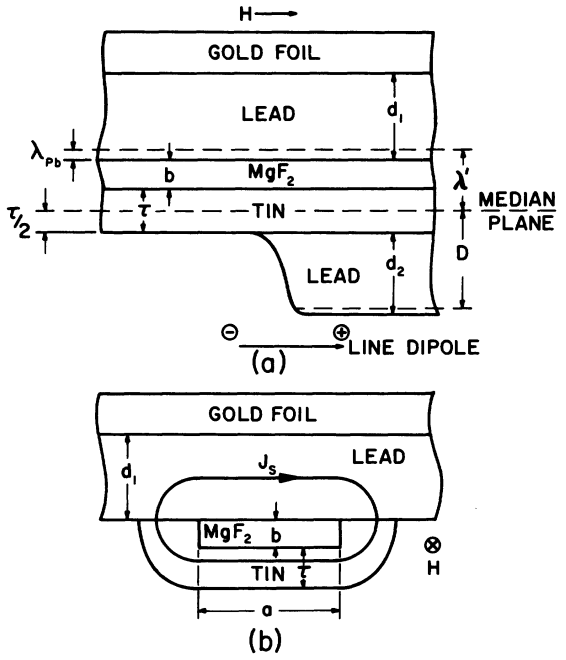

FIG. 9. (a) Schematic of the right-half cross section through the length of the sample. The line dipole is made of two copper wires running parallel to each other and width of the sample and perpendicular to the plane of the paper. d_1, b, τ, and d_2 are the film thicknesses of base film of lead, insulating layer of MgF_2, tin, and guard films of lead, respectively. (b) Schematic of cross section through the center of the sample perpendicular to its axis. This cross section is perpendicular to the one in (a) and indicates the supercurrent path by the loop with arrow head. The lead guard films do not show in this cross section since they are present only at the ends.

ducting, then the signal would originate entirely from the step due to the flux expelled from the lead guard films. In this case the signal would increase linearly with field as shown by the curve OAB; dropping discontinuously to zero when the field becomes greater than $H_{c,Pb}$. When the tin film is in the superconducting state it partially expels the applied flux. The step of the expelled flux at the junction p thus decreases, reducing the signal accordingly. The signal varies linearly with field at low values as expected theoretically and shown by the curve OA_1. If the applied field is increased further two things can happen. One, the tin film becomes normal discontinuously at the field H_{A1}; in this case the signal jumps for A_1 to the point A_2 on OAB curve. This is a first-order transition of the superconducting tin film to the normal state. Two, the signal starts increasing nonlinearly but smoothly beyond H_{A1} reaching the point A above which it again shows linear dependence on the applied field ($H < H_{c,Pb}$). This corresponds to a continuous second-order transition to the normal state. We have observed the latter case for all the four samples. At 1.96 °K for sample 4 and 2.30 °K for sample 2 we have observed the first case. The confirmation that the signal at higher fields is entirely due to the lead films was obtained by taking data above $T_{c,Sn}$ in each case. The slope of the line through the data points at low-field values in Figs. 7 and 8 is smaller than that at higher fields, indicating the diamagnetism of the tin film. This slope becomes smaller and H_A becomes larger as the temperature of the sample is decreased below $T_{c,Sn}$, as expected theoretically.

The experimental data can be further analyzed to obtain (i) depairing curves, i.e., the current density J_s versus the vector potential A curves; (ii) the critical vector potential A_c at which the supercurrent becomes zero due to the complete depairing in the tin film; and (iii) London's penetration depth in tin films. The critical vector potential A_c can be easily calculated from the value of the applied magnetic field at point A in Fig. 10 where the supercurrent in the tin film reduces to zero.

To obtain the desired supercurrent density J_s versus the vector potential A (the depairing curves) from the experimental data we proceed as follows. The vector potential A is related to flux ϕ, the quantity measured in the experiment, by the relationship

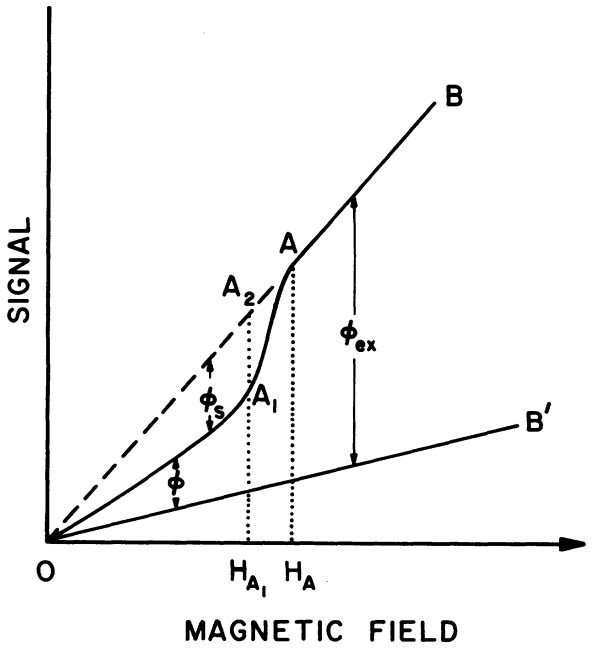

FIG. 10. Expected signal from the electronics for a sample as a function of external magnetic field at a constant temperature. This illustration is used to explain the experimental data.

$$\oint \vec{A} \cdot d\vec{l} = \oint \oint \vec{H}_{in} \cdot d\vec{S} = \phi \,, \tag{15}$$

where the line integral over A is taken over the path of J_s shown in Fig. 9(b). The surface integral integrates the magnetic field over the surface enclosed by the line integral obtaining the flux ϕ enclosed by supercurrents passing through the tin sample. Because of the finite thickness of the tin film, the vector potential and thus the supercurrent vary somewhat across the film thickness. In all samples except for perhaps sample 3 at its lowest temperature, the film thickness is appreciably less than the penetration depth so that the vector potential variation across the film is linear. The average value of A in the tin sample thus occurs halfway through its thickness, the median plane of Fig. 9(a). The line integral in (15) is chosen to pass through the middle of the thickness of the tin sample so that the average value of A is determined in (15). The path through the lead-base film is chosen to be deeper than the penetration depth so that the contribution to (15) from the Pb film is a constant independent of temperature. We choose that constant to be zero.

An average value for H_{in} can be defined from (15) by

$$H_{in} a\lambda' = A(a + 2\lambda') \,, \tag{16}$$

where

$$\lambda' = \tfrac{1}{2}\tau + b + \lambda_{Pb} \,,$$

and a is the width of the insulating region. The quantity λ' is the effective thickness of the region through which H_{in} penetrates. The quantities defining λ' are shown in Fig. 9(a). The quantity a is typically $\frac{3}{4}$ mm and is thus much larger than λ' $\sim 10^{-5}$ cm, permitting (16) to be simplified to

$$A = H_{in}\lambda' = \phi/a \,, \tag{17}$$

where, again, A is the value of the vector potential at the median plane of the tin sample. From (17) we note that ϕ is proportional to the vector potential A. Since the experimental signal is produced by fluxes, it will be convenient in our analysis of the data to relate everything to the appropriate flux which can be then easily related to A when necessary.

In order to obtain the desired results of J_s vs A, one must extract those parts of the signal which are proportional to the flux ϕ_s expelled and the flux ϕ enclosed by the tin sample. As shown in (17) ϕ is proportional to A, while applying (7) along the path shown in Fig. 9(b), we obtain ϕ_s proportional to J_s:

$$\phi_s = J_s 4\pi\tau a\lambda' , \tag{18}$$

where we used the fact that $L = 4\pi\tau a\lambda'$ for our sample configuration.

It is straightforward to get that part of the signal which is proportional to the expelled flux ϕ_s by taking the difference between the signals corresponding to the curves OAB and OA_1AB in Fig. 10. The signal corresponding to the curve OAB is directly proportional to the flux contained within the sample when the tin film is not superconducting while the curve OA_1AB is proportional to the flux when the tin film is superconducting.

To obtain that part of the signal which is proportional to ϕ is more difficult, because of the extra contribution of the lead guard films to the flux step p.

This extra signal must be subtracted from the total signal (the curve OA_1AB) before the remainder can be interpreted as giving information about only the tin film. This correction can be carried out by calculating the part of the step height contributed by the lead guard films. Referring to Fig. 9(a), we note that the lead guard film expells flux from the thickness $D = (\frac{1}{2}\tau + d_2 - \lambda_{Pb})$ beyond the median plane of the tin sample. The curve OAB in Fig. 10 is proportional to the flux expelled from the thickness $D + \lambda'$. The signal proportional to the unwanted additional flux expelled by the guard films is given by the straight line OB′ in Fig. 10 with a slope

$$\text{slope of OB}' = \frac{D}{D + \lambda'} \text{ (slope of OB')} \,. \tag{19}$$

The difference between the measured curve OAB and OB′ is proportional to ϕ, the flux enclosed by the tin sample.

To make the plot of the ϕ_s-vs-ϕ curve more accurate, the various subtractions are carried out at the data points rather than using a smooth curve. Signals corresponding to the lines OAB and OB′ are evaluated using straight-line equations. All the points of ϕ_s vs ϕ obtained as described above are then plotted and a smooth curve is drawn through these points to give the required depairing curve. The curves ϕ_s vs ϕ for sample 4 are shown in Fig. 11. Figures 12–15 show the depairing curves for all the samples; however, here ϕ_s-vs-ϕ curves have been converted into the current density J_s versus the vector potential A using Eqs. (17) and (18). These curves (except those for sample 4 at 1.96 °K and sample 2 at 2.30 °K) show that J_s increases linearly for small values of A, reaches a maximum value where it clearly shows departure from linear behavior on either side of the maximum, then starts decreasing gradually and nonlinearly at higher values of A, and finally becomes zero at a critical value of A_c. The finite slope of the curve at A_c confirms the second order transition in tin films as predicted by the theory. The values of A_c are listed in Table II for each sample investigated. The comparison with theoretical val-

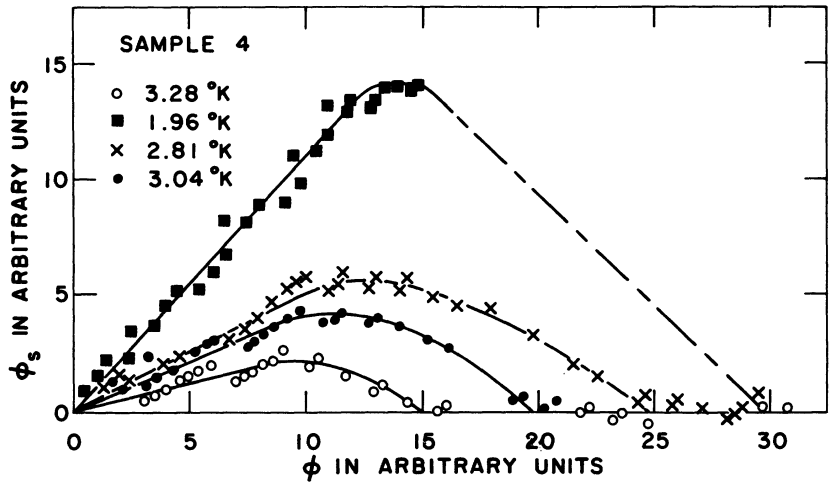

FIG. 11. ϕ_s-vs-ϕ curves for sample 4 at 1.96 °K, 2.81 °K, 3.04 °K, and 3.28 °K. The dot-dashed curve represents the first-order transition and has slope of -1.

ues will be made in Sec. V.

The J_s-vs-A curves for sample 2 at 2.30 °K (Fig. 13) and sample 4 at 1.96 °K (Fig. 15) also show a linear relation between J_s and A at low values of A and a small nonlinear region near the maximum of J_s but, because of the bad load line, the rest of the nonlinear region is not observable, and instead, a first-order transition occurs as shown by the dot-dashed line. It has been said before that the abrupt transition in these two samples is a first-order transition. The strongest support that this first-order transition is caused by a bad load line comes from the consideration of the load line which is given by Eq. (9), where $\phi_{ex} = H\lambda' a$ is the total of the externally applied flux through the tin sample. A sharp transition, which will occur in a bad load line situation, should take place via the load line; that is, the slope of the dot-dashed line must be the same as that of the load line. The slope of the load line in a plot of ϕ_s-vs-ϕ for constant ϕ_{ex} is -1, as seen from Eq. (9). Therefore the slope of the dot-dashed line in Fig. 11 must be -1 if it is to represent a first-order transition. This is indeed the case in Fig. 11 as well as for the sharp transition in sample 2 at 2.30 °K. This check confirms that the observed sharp transitions in sample 2 and sample 4 are first order and are caused by a bad load line.

London's penetration depth λ in tin films as indicated by Eqs. (8) and (10) is obtained by the initial slope of the depairing curves. This slope is defined as

$$\gamma^{-1} = \lim_{\phi \to 0} (\phi_s/\phi) ,$$

and since $\gamma = \lambda^2/\tau\lambda'$,

$$\lambda^2 = \tau\lambda'/\lim_{\phi \to 0} (\phi_s/\phi) . \qquad (20)$$

TABLE II. Important parameters deduced from the experimental data.

Sample	T (°K)	$t = T/T_c$	γ	λ (Å)	H_c (Oe)	$10^{-3} A_c$ (Oe cm)	λ/τ	A_c/A_m
1	2.44 ± 0.01	0.63 ± 0.012	1.48 ± 0.10	880 ± 50	156.9 ± 10	1.61 ± 0.13	1.72	2.00
1	3.02 ± 0.01	0.78 ± 0.015	4.44 ± 0.20	1619 ± 85	136.7 ± 10	1.40 ± 0.13	3.16	1.40
1	3.52 ± 0.01	0.91 ± 0.018	6.70 ± 1.0	1982 ± 175	112.1 ± 10	1.15 ± 0.12	3.87	1.60
2	2.30 ± 0.01	0.596 ± 0.005	0.65 ± 0.04	1363 ± 50	103.6 ± 3[a]	1.26 ± 0.05	1.27	
2	2.80 ± 0.01	0.725 ± 0.005	1.25 ± 0.08	1890 ± 65	101.6 ± 3	2.48 ± 0.09	1.80	2.12
2	3.10 ± 0.01	0.803 ± 0.007	2.2 ± 0.20	2508 ± 120	79.7 ± 2	2.16 ± 0.06	2.38	1.58
2	3.64 ± 0.01	0.945 ± 0.005	8.5 ± 1.5	4929 ± 600	41.8 ± 2	1.13 ± 0.06	4.54	1.55
3	1.78 ± 0.03	0.468 ± 0.010	2.1 ± 0.15	1137 ± 50	167.4 ± 5	2.55 ± 0.09	2.81	1.68
3	2.24 ± 0.02	0.589 ± 0.008	3.0 ± 0.25	1358 ± 65	149.5 ± 5	2.24 ± 0.08	3.41	1.58
3	3.15 ± 0.01	0.829 ± 0.007	6.7 ± 1.0	2030 ± 160	109.6 ± 3	1.64 ± 0.05	4.94	1.55
4	1.96 ± 0.03	0.516 ± 0.010	0.95 ± 0.02	1247 ± 25	97.6 ± 3[a]	1.37 ± 0.05	2.20	
4	2.81 ± 0.02	0.739 ± 0.009	2.1 ± 0.2	1853 ± 90	81.7 ± 3	2.33 ± 0.06	3.20	1.85
4	3.04 ± 0.01	0.800 ± 0.006	2.3 ± 0.4	1961 ± 170	67.7 ± 2	1.92 ± 0.05	3.42	1.73
4	3.28 ± 0.01	0.863 ± 0.008	4.0 ± 1.0	2558 ± 325	51.8 ± 2	1.48 ± 0.05	4.46	1.62

[a]The value of H_c is not for the complete depairing but is the value where the sharp transition takes place.

The values of λ for each sample at various reduced temperatures $t = T/T_c$ are listed in Table III.

V. DISCUSSION

In this section we discuss the experimental results on samples 2–4, and compare them with the theoretical predictions. Because of a large uncertainty in the film thickness determination in sample 1, a quantitative comparison of its results is not very meaningful and therefore will not be done here. Finally we discuss recent work of Schmidt[16] and of Hansen *et al.*,[17] which calculate the effect of fluctuations on the depairing behavior as discussed by Fulde and Ferrell.[5]

A. Penetration Depth of Magnetic Field in Tin Films

The values of the penetration depth λ_{Sn} of a magnetic field into tin films in various samples at different temperatures are listed in Table II. These values are deduced from the initial slope of the depairing curves, i.e., ϕ_s-vs-ϕ curves, as given by Eq. (20). The uncertainty determining the quantity γ, which is the $\lim_{\phi\to 0}(\phi_s/\phi)^{-1}$, is 1–10% depending upon its value. This error results owing to a large scatter in data at low values of ϕ. The present accepted value of λ_{Sn} for bulk tin is 510 Å at 0 °K. Comparing this value with the values of λ_{Sn} listed in Table II, one finds that the experimentally deduced values of λ_{Sn} are much larger than 510 Å. This is due to the dependence of λ on the temperature and electron mean free path l. Following Tinkham,[28] one can write

$$\lambda(t, l) = \lambda(0, \infty)(1 - t^4)^{-1/2}(1 + \xi_0/l)^{1/2}, \qquad (21)$$

where $\lambda(t, l)$ is the penetration depth at temperature $t = T/T_c$, and electron mean free path l; $\lambda(0, \infty)$ is the penetration depth at $T = 0$ °K, and infinite electron mean free path; and ξ_0 is the temperature independent BCS coherence length. Thus, the shorter the mean free path, the larger is the penetration depth. Since the quantity γ is proportional to λ_{Sn}^2, it varies as $(1 - t^4)^{-1}$ with temperature. γ is plotted against $(1 - t^4)^{-1}$ in Fig. 16 for samples 2–4, which shows that the theoretical temperature dependence of γ is obeyed within experimental accuracy. A straight line is drawn through the data points for each sample and extrapolated to $t = 0$, that is, $T = 0$ °K, to give the value of λ at 0 °K for each sample. $\lambda(0, l)$ and l are then calculated using Eqs. (20) and (21), respectively, and are listed in Table III. Values of l for samples 3 and 4 indicate that the major scattering in these samples is due to the surface, since l is of the order of the film thickness. In sample 2 the bulk scattering is dominant, since λ is appreciably smaller than the film thickness. An independent measurement to check the values of l deduced from Eq. (21) could not be made because of the complicated geometry of the samples.

TABLE III. Penetration depth, mean free path, and coherence length in tin films.

Sample	$\gamma(0)$	$\lambda(0, l)$ (Å)	l (Å)	ξ_0 (Å)	Range of $\xi(T)$ (Å)
2	0.50 ± 0.05	1196 ± 80	511 ± 80	2100	1386–5852
3	2.10 ± 0.05	1137 ± 53	618 ± 65	2100	1327–2342
4	0.80 ± 0.05	1144 ± 62	570 ± 77	2100	1337–2513

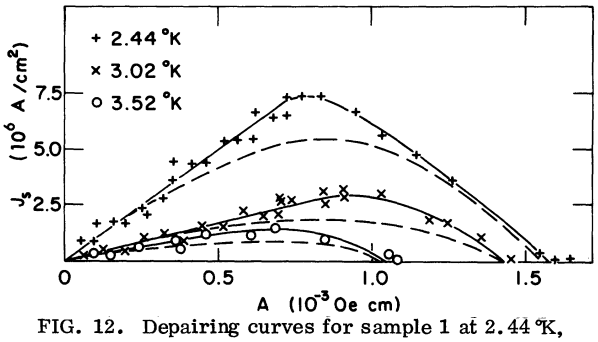

FIG. 12. Depairing curves for sample 1 at 2.44 °K, 3.02 °K, 3.52 °K. The dashed curves are as predicted by the GL theory.

To get an approximate estimate of the uniformity of the supercurrent density and the vector potential across the film thickness a knowledge of (λ_{Sn}/τ) is required. These values are also listed in Table II. It should be noted that this ratio is 1.27 and 1.80 for the tin film in sample 2 at the reduced temperatures $t = 0.596$ and $t = 0.725$, respectively. Therefore the thin film approximation, which requires (λ/τ) to be at least 2, is only approximately fulfilled. Samples 3 and 4 do satisfy this condition at all temperatures at which data were taken. Therefore the theoretical assumption that the current density varies linearly in the film is fulfilled in these two samples and is approximately valid for sample 2.

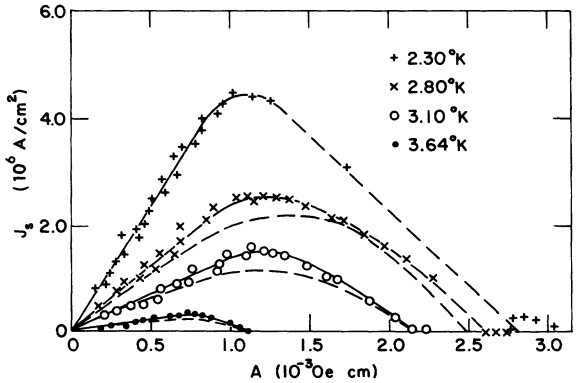

FIG. 13. Depairing curves for sample 2 at 2.30 °K, 2.80 °K, 3.10 °K and 3.64 °K. Dashed curves are as predicted by the GL theory. The dashed straight line represents the first-order transition.

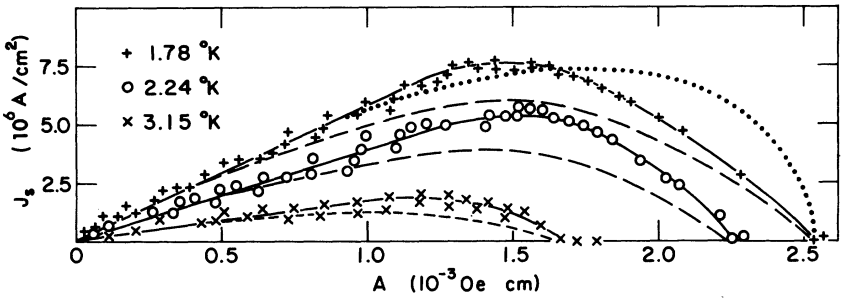

FIG. 14. Depairing curves for sample 3 at 1.78 °K, 2.24 °K, and 3.15 °K. Dashed curves are as predicted by the GL theory. The dotted curve is the Maki theory at 0 °K.

Another theoretical assumption in deriving Eq. (1) is that the film thickness is smaller than the temperature dependent Ginzburg–Landau coherence length $\xi(T)$, so that the order parameter be spatially independent. This can be checked by use of the relation[29]

$$\xi(T) = 0.85(\xi_0 l)^{1/2}(1-t)^{-1/2} . \tag{22}$$

The calculated values are listed in Table III and show that the condition $\tau < \xi(T)$ is satisfied for all the samples at all temperatures at which data were taken.

Douglass[30] has shown that the penetration depth of a magnetic field in a thin superconducting film depends upon the applied field. This dependence is given by the following equation:

$$\lambda(t, l, H) = \lambda(t, l, 0)[1 - (H/H_{c1})^2]^{1/2} , \tag{23}$$

where H is the parallel field applied to the both sides of the film,

$$H_{c1} = \sqrt{24}\,\lambda(t, l, 0)\tau^{-1}H_{cb}(t) , \tag{24}$$

and $H_{cb}(t)$ is the thermodynamic critical field. To estimate the change in λ_{Sn} with the field consider the data for sample 3 at 1.78 °K for which $(\lambda_{Sn}/\tau) \simeq 3$. The change in λ_{Sn} at the maximum field of 167 Oe is then calculated to be approximately 0.1% and is negligible compared to the observed change in the depairing regime.

B. Depairing Curves

The comparison of the shape of the depairing curves, i.e., current density J_s versus vector potential A inside the thin tin films, shown in Figs. 12–15, is made with Ginzburg–Landau expression [Eq. (4)]:

$$J_s = N_s e A(1 - A^2/A_c^2) .$$

The theoretical curves are shown by the dashed curves along with the experimental curves. The agreement between these is reasonably good. Maki[6] has also calculated a theoretical relation between J_s and A, which reduces to the Ginzburg–Landau expression near T_c. For comparison Maki's calculated curve at 0 °K is also shown in Figs. 14 and 15 at the lowest temperature curves obtained experimentally. The theoretical curves are normalized to have the same initial slope and A_c as the experimental curves. The Ginzburg–Landau theory is not expected to fit better than observed for it is expected to work best near the transition temperature. This, indeed, is observed to be true. Maki's curve at 0 °K displays a very poor agreement with the experimental curves ob-

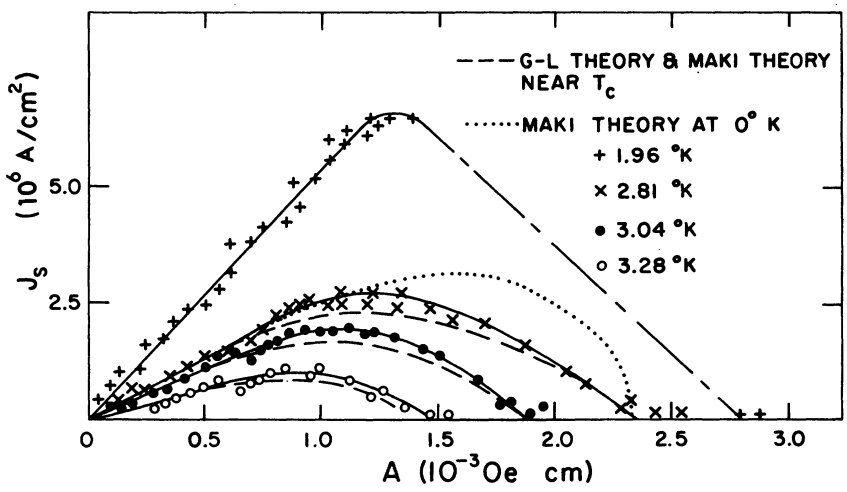

FIG. 15. Depairing curves for sample 4 at 1.96 °K, 2.81 °K, 3.04 °K and 3.28 °K. Dashed curves are as predicted by the GL theory. The dotted curve is the Maki theory at 0 °K. The dot-dashed curve represents the first-order transition.

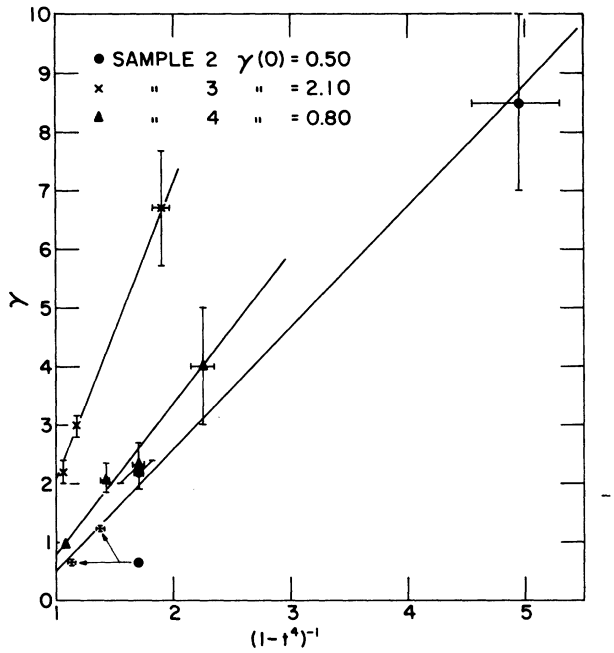

FIG. 16. Reciprocal slope of ϕ_s-vs-ϕ curves, given by γ, in the limit $\phi \to 0$ are plotted as a function of $(1-t^4)^{-1}$, where $t = T/T_c$.

tained at the lowest temperature at which data was taken. This lack of agreement is not surprising as Maki's calculations assume the extremely dirty limit, that is, $l/\xi_0 \ll 1$, while this ratio is approximately $\frac{1}{3}$ for the tin film in sample 3 at the lowest temperature of 1.78 °K, which is also appreciably greater than 0 °K.

One of the obvious departures from the Ginzburg–Landau theory is that the experimental curves appear to retain their linearity to higher fields than the theory predicts, and then a relatively sharp depairing region sets in. The experimental curves also show that the maximum of the curves becomes broader as one approaches the transition temperature. This is expected theoretically. In general one expects the maximum of the curves to be broader owing to electron scattering at the boundaries, and other effects, namely, impurities, than predicted by the theory. The effect of magnetic field on the energy gap and the penetration depth, if it becomes appreciable, may also modify the shape of the depairing curve near its maximum. However, the magnetic fields used in this work are too small to make this effect appreciable.

It should also be noted that for observing the complete depairing regime in the reported experiments here, one requires $\gamma \geq 2$ as predicted by the Ginzburg–Landau theory. This condition is not fulfilled for sample 2 at 2.30 °K and sample 4 at 1.96 °K, where a first-order transition is observed. In sample 2 at 2.80 °K, we seem to observe only part of the depairing regime. The lower part of the curve near A_c indicates a first order transition. This part of the curve shows a slope of -1, the condition necessary for the abrupt transition. We have drawn the theoretical curve in this case using a value of A_c which gave the best agreement with the experimental curve. The value of A_c which is listed in Table II for this temperature is the one which we have used to fit the theoretical curve with the experimental curve.

Thus, most of our data confirm the general features of the GL theory and show that under appropriate experimental conditions supercurrent should gradually decrease to zero after reaching a maximum indicating a gradual decrease in the order parameter and finally a second-order phase transition.

C. Critical Vector Potential

The values of the critical vector potential deduced from the experimental data are listed in Table II and again in Table IV along with the theoretical calculated values. Early works of Rogers,[2] Bardeen,[3] and Paramenter[4] showed that a current flow through a superconductor provides a depairing mechanism once the pairing momentum exceeds the so-called depairing momentum (Δ_0/V_F) at 0 °K, where $2\Delta_0$ is the energy gap in absence of a current flow ($q = 0$ and $T = 0$ °K) and V_F is the Fermi velocity. The theory predicted the current to reach a maximum when the total momentum of the electron pairs reaches the value $1.03\,(\Delta_0/V_F)$, and beyond which the current decreases monotonically to zero at $q = q_c = 1.36\,(\Delta_0/V_F)$. Ginzburg–Landau theory predicts a different current dependence on q as given by (4) although the qualitative features remain the same. The Ginzburg–Landau theory predicts a maximum of current when $q = 3^{-1/2} q_c$, where

$$q_c = \frac{\sqrt{3}\,\Delta_0}{V_F}\left(\frac{1-t^2}{1+t^2}\right)^{1/2}$$

is the pair momentum at which the current decreases to zero. Both of these calculations ignore

TABLE IV. Comparison of the observed critical vector potential with theory.

Sample	Reduced temperature t	Observed A_c (10^{-3} Oe cm)	A_c predicted by GL theory (10^{-3} Oe cm)	A_c predicted by Maki theory (10^{-3} Oe cm)
2	0.725	2.48	0.85	2.52
2	0.803	2.16	0.70	2.17
2	0.945	1.13	0.36	1.16
3	0.468	2.55	1.19	3.05
3	0.589	2.24	1.04	2.77
3	0.829	1.64	0.64	1.81
4	0.739	2.33	0.80	2.42
4	0.800	1.92	0.70	2.13
4	0.863	1.48	0.57	1.61

the effect of collisions on the penetration depth.

Simple Ginzburg–Landau theory can be modified to include collision effects; however, we compare our results with those of Maki,[6] who has also studied the current carrying state of a superconductor with the aid of Green's function technique in the limit $l/\xi_0 \ll 1$. He found that q_c at 0 °K can be determined by the relation

$$\zeta \frac{\Delta}{\Delta_0} = \frac{2}{3} \frac{\tau (q V_F)^2}{\Delta_0 \hbar} , \tag{25}$$

where τ is the collision time which is approximately equal to (l/V_F), where l is the electron mean-free path, $2\Delta_0$ is the energy gap at $T = 0$ °K and $q = 0$, Δ is the order parameter, and $\zeta\Delta/\Delta_0$ is a temperature-dependent constant which is equal to $\frac{1}{2}$ at zero temperature. Thus, Maki predicts that

$$q_c(T=0) = \left(\frac{3\hbar\Delta_0}{4\tau V_F^2}\right)^{1/2} \tag{26a}$$

and, therefore,

$$A_c(T=0) = \frac{c}{e}\left(\frac{3\hbar\Delta_0}{4\tau V_F^2}\right)^{1/2} \tag{26b}$$

for a dirty superconductor. Relation (26b) explicitly includes the effect of finite l on A_c.

To make a quantitative comparison of the observed values of A_c (A_{c0}) and those calculated from Maki's theory (A_{cm}), one must use Eq. (25), where a temperature dependence of $\zeta\Delta/\Delta_0$ can be included. Maki[6] has calculated expressions for the current as a function of q only for zero temperature and $T/T_c = 0.8$. It is tedious to derive a temperature dependence of $\zeta\Delta/\Delta_0$ from his calculations. In order to get this temperature dependence we take advantage of the work of Maki and Fulde[9] who have shown the equivalence of the current case to the case of paramagnetic impurities in a superconductor. This allows us to use all of the numerical work done for the paramagnetic impurity case by Skalski *et al.*,[31] who have calculated the paramagnetic impurity dependence on T_c, order parameter, and energy gap of a superconductor. Thus we can identify temperatures below T_c in the current case as the depression in T_c due to paramagnetic impurities, and $\zeta\Delta/\Delta_0$ as $\Gamma/\Delta^P(0)$ where Γ is the inverse of the collision time in the presence of the impurities, and $\Delta^P(0)$ is the order parameter at zero temperature in the absence of the impurities. In this way we calculate the values of $A_{cm}(T)$ listed in Table IV. To obtain these values we used the values of l listed in Table III, $V_f = 0.67 \times 10^8$ cm/sec and $2\Delta_0 = 3.52 k_b T_c$, where k_b is the Boltzmann constant. A comparison of the calculated and the observed values of A_c shows a good agreement between the two for sample 2, but increasingly poorer agreements for samples 4 and 3. From mean-free-path measurements as listed in Table III compared to the film thicknesses, we note that the samples in better agreement with Maki's theory are those that also agreed better with his assumption of being "dirty." Table IV also lists calculated values of A_c in the GL theory. The agreement between the GL theory and the experiment is seen to be poor for all samples, which is not surprising since the effect of collisions on penetration depth is not included in the theoretical expression for q_c. However, it is worthy of note that the measured A_c are between the Maki and GL limits in an order that is consistent with how "dirty" they are. Other factors which will effect A_c are the anisotropy of the energy gap and the Fermi velocity, and magnetic field dependence of the energy gap since the film is also affected by an average field $\frac{1}{2}(H_{ex} + H_{in})$ in addition to the supercurrent which is determined by $H_{ex} - H_{in}$. The magnetic field effect can be shown to be negligibly small in our case from the results of Douglass.[32]

The temperature dependence of A_c in the Ginzburg–Landau theory, which Maki's theory also reduces to near T_c, is given by $(1-t^2)^{1/2}(1+t^2)^{-1/2}$. Observed values of A_c are plotted in Fig. 17 as a function of $(1-t^2)^{1/2}(1+t^2)^{-1/2}$. It is seen that A_c obeys the theoretical temperature dependence reasonably well.

The values of the vector potential at which the discontinuous transition takes place are 1.26×10^{-3} Oe cm for sample 2 and 1.37×10^{-3} Oe cm for sample 4. These values can be compared with the corresponding theoretical value of the vector potential A_s at which the depairing of the Cooper pairs sets in. This is given by $\sim(\Delta/V_F)$. The cal-

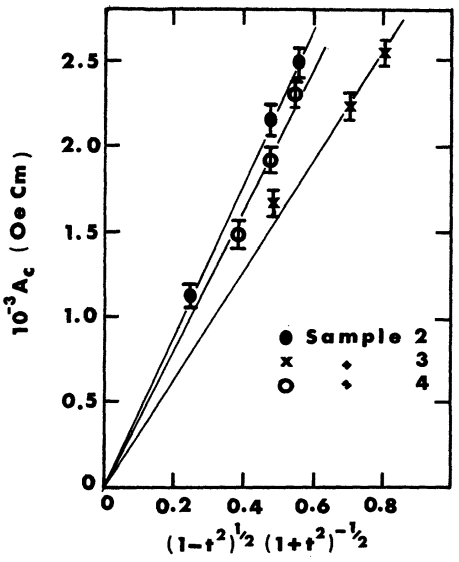

FIG. 17. Critical vector potential A_c are plotted as a function of $(1-t^2)^{1/2}(1+t^2)^{-1/2}$, where $t = T/T_c$.

culated value of A_s is found to be 0.9×10^{-3} Oe cm at zero temperature. The observed values of the vector potential for the discontinuous transition (Table II) are, thus, reasonable since we expect these to be higher than the calculated values of A_s; the actual value of the vector potential for the sharp transition occurrence will depend upon the shape of the depairing curve and the load line.

The ratio of the vector potentials at which the complete depairing occurs is also of interest in the theory. This ratio is 1.73 in the Ginzburg–Landau theory and experimental values are listed in Table II as A_c/A_m.

The maximum current density J_{sm} for tin films is plotted in Fig. 18 as a function of $(1-t^2)(1-t)^{1/2}$, the temperature dependence of J_{sm} predicted by the GL theory. The agreement is observed to be good. We should also mention that the observed values of J_{sm} are found to be larger than previously reported in similar experiments, and are of magnitude expected theoretically.

D. Fluctuation Effects

There have been recent criticisms of the theoretical analysis of the observability of the negative self-inductance region occurring for A values larger than A_m where the current reaches its maximum J_{sm}. Schmid[16] and Hansen *et al.*[17] have argued that this negative self-inductance region is unstable with respect to fluctuations and thus cannot be observed experimentally except in a microstrip all of whose dimensions are smaller than the coherence length. Since our paper claims to observe this region for a much larger sample it is important to try to resolve this discrepancy. Our criticism of the work of Schmid[16] and Hansen *et al.*,[17] is based on both theoretical and experimental grounds.

The theoretical analysis of fluctuations neglected the effects of the long-range electrostatic forces induced by the charge density associated with the fluctuations. This neglect can conceivably completely negate the conclusions of Refs. 16 and 17, and until this deficiency is corrected one cannot draw any conclusions from the analysis. The sample configurations considered in Refs. 16 and 17 differ from the one used in this experiment in several important respects. The sample configuration used in the theoretical analysis was an isolated strip through which a uniform current is passed. Our experimental sample was placed in proximity to a lead superconducting plane and had lead superconducting guard rings at each end. Any fluctuation in the sample would induce a response from these lead regions shielding the fluctuation from them. How this would then react back on the fluctuation itself must be analyzed before any conclusion about the stability of the fluctuation can be drawn.

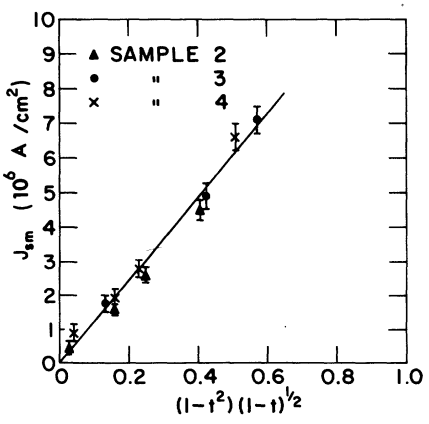

FIG. 18. Maximum supercurrent density J_m is plotted as a function of $(1-t^2)(1-t)^{1/2}$, where $t=T/T_c$.

However, the clearest evidence for the reality of the negative self-inductance region is experimental. We have carefully looked experimentally for other effects which might have given rise to the observed decrease in supercurrent for increasing magnetic field and found none. These are (i) the possibility of an intermediate state, namely, the tin film transformed into normal and superconducting regions and therefore the transition did not take place uniformly over the whole length of the tin film; (ii) the experimental apparatus introduced the nonlinearity in some manner; or (iii) the tin film gradually allowed the penetration of the applied magnetic field by forming fluxoids as in a type-II superconductor.[33]

The sample configuration used in this experiment was specifically designed to prevent the formation of an intermediate state. The superconducting Pb base guaranteed that the external magnetic field will be precisely parallel to the tin sample. The Pb guard rings at the ends of the sample eliminate the possibility of the formation of an intermediate state at the sample ends. Nowhere in the experiment is any part of the sample while superconducting subjected to a magnetic field near its critical value. The configuration of a plane geometry with the magnetic field parallel to the plane does not permit of any demagnetizing factor that could lead to an intermediate state.

The data clearly show that the observed nonlinearity was not introduced by the experimental apparatus. The sharp transitions observed in samples 2 and 4 at the bad load-line conditions indicate the smearing introduced by the apparatus. As can be seen in Fig. 8, this experimental smearing is much less than the widths of the nonlinear regions in the good load-line condition. A study was made to determine the cause of the small experimental smearing of the sharp transitions. It was found

that the smearing was caused by the amplitude of the dipole driving field at the sample. Decreasing this amplitude sharpened the transition even further, but in all cases the experimental smearing produced negligible distortion of the nonlinear region in the good load-line condition.

The possibility of fluxoid penetration was checked in various ways. Possible hysteresis effects were checked in sample 3. We did not observe any hysteresis in the observed behavior of the tin film when the field was reduced before reaching a complete transition to the normal state. However, if the field was increased beyond the field where the tin film reached a complete transition, and then decreased, all at 1.76 °K, a curve was obtained which was exactly similar to the original curve except that it was shifted to the right-hand side on the magnetic field axis. At higher temperatures no hysteresis whatsoever was found. Further details of the hysteresis in sample 3 are given in Ref. (11). We did not investigate in full detail to determine why flux was trapped while the sample was in the magnetic field induced normal state at 1.76 °K but not at higher temperatures because that was not the goal of this measurement,[11,34] but it is clear that these results make fluxoid penetration highly unlikely as a cause of the nonlinear region. One would expect a hysteresis to become apparent as soon as fluxoids penetrated into the tin sample. The fact was that no hysteresis ever appeared until the normal state was reached.

To further check against the possibility of fluxoid penetration, the shape of the experimental curves was measured using two different spacing of the driving dipoles. This was done by having three copper wires closely spaced for each dipole driver. Alternating current could be passed through any pair of wires. Two sets of data were taken for sample 2 using dipoles having approximate spacings of 0.008 and 0.012 in. The 0.012-in. dipole samples a larger region of the tin than that by the 0.008-in. dipole, and therefore the former is expected to give information averaged over a larger length of the film. The shape of the nonlinear region remained unaltered for both driving dipoles. If fluxoid penetration were taking place, one would expect that this penetration occurs throughout the sample. The larger dipole would sense more of the fluxoids and measure a different (smaller) apparent flux step than the smaller dipole. This difference would be large enough to be easily seen by the apparatus if present. The fact that no difference was seen indicates that the flux step is occurring only in the region where the tin sample meets the Pb guard ring and nowhere else along the sample. This is consistent with depairing but not consistent with fluxoid penetration.

Perhaps the strongest evidence that our interpretation is correct is the positive ones that all of the observed phenomena are explainable by it; the good and bad load-line behavior, including the transition between the two at the slope of -1 in the ϕ_s-vs-ϕ plot; the comparison between measured and calculated values of A_c; the measured shape of the depairing curves; the large values of J_{sm}, etc.

VI. CONCLUSION

We have reported in this paper the first detailed study of supercurrent in thin tin films as a function of an external magnetic field. In order to observe theoretically predicted decrease in supercurrent induced by depairing we investigated samples having small self-inductances and observe the gradual decrease to zero of supercurrent from its maximal value which we show to be due to depairing in thin tin films. By investigating samples which could change from having a first to a second order superconducting transition, we have also confirmed that the slope of the load line is of prime importance if the complete depairing regime is to be accessible to experimental observation. We believe this to be the first experimental investigation in which the complete depairing regime, induced by a dc current, has been observed. A quantitative comparison of the theory and the experimental results is found to be reasonably good.

ACKNOWLEDGMENTS

We would like to express our sincere thanks and gratefulness to Professor Richard A. Ferrell for his continual interest in the experiment, and for many enlightening and helpful discussions. Thanks are also due Dr. P. Fulde for helpful communications. One of us (E. A. S.) would like to acknowledge an enlightening conversation with Dr. Patrick Lee. The aid of Professor R. I. Gayley in developing the equipment and the continual interest of Professor J. R. Anderson are gratefully acknowledged.

---

*Based on the thesis submitted by Anil K. Bhatnagar to the Faculty of the Graduate School of the University of Maryland in partial fulfillment of the requirements for the degree of Doctor of Philosophy, 1968.

[1]V. L. Newhouse, *Applied Superconductivity* (Wiley, New York, 1964).

[2]K. T. Rogers, Ph.D. thesis (University of Illinois, 1960) (unpublished).

[3]J. Bardeen, Rev. Mod. Phys. **34**, 667 (1962).

[4]R. H. Paramenter, RCA Rev. (Radio Corp. Am.) **26**, 323 (1962).

[5]P. Fulde and R. A. Ferrell, Phys. Rev. **131**, 2457 (1963).

[6]K. Maki, Prog. Theor. Phys. **29**, 333 (1963); Prog. Theor. Phys. **29**, 603 (1963).

[7]L. N. Cooper, Phys. Rev. **104**, 1189 (1956).
[8]J. Bardeen, L. N. Cooper, and J. R. Schrieffer, Phys. Rev. **108**, 1175 (1957).
[9]K. Maki and P. Fulde, Phys. Rev. **140**, A1586 (1965).
[10]M. A. Woolf and R. Reif, Phys. Rev. **137**, A557 (1965); D. K. Finnemore, D. L. Johnson, J. E. Ostenson, F. H. Spedding, and B. J. Beaudry, Phys. Rev. **137**, A550 (1965); J. J. Hauser, H. C. Theuerer, and N. R. Werthamer, Phys. Rev. **142**, 118 (1966).
[11]A. K. Bhatnagar and E. A. Stern, Department of Physics and Astronomy Technical Report No. 755, University of Maryland, 1967 (unpublished).
[12]A. K. Bhatnagar and E. A. Stern, Phys. Rev. Lett. **21**, 1061 (1968).
[13]A. K. Bhatnagar, Bull. Am. Phys. Soc. **14**, 191 (1969).
[14]O. P. Hansen, Phys. Rev. **181**, 671 (1969).
[15]R. P. Groff and R. D. Parks, Phys. Rev. **176**, 567 (1968).
[16]A. Schmid, J. Low Temp. Phys. **1**, 13 (1969).
[17]E. Brun Hansen and P. Voetmann Christiansen, University of Copenhagen, Denmark, 1970 (report of work prior to publication); P. V. Christiansen, E. B. Hansen, and C. J. Sjöström, J. Low Temp. Phys. **4**, 349 (1971).
[18]V. L. Ginzburg and L. D. Landau, Zh. Eksp. Teor. Fiz. **20**, 1064 (1950).
[19]C. D. Mitescu, Rev. Mod. Phys. **36**, 305 (1964); also, in *Proceedings of the Tenth International Conference on Low-Temperature Physics, Moscow, 1966*, edited by M. P. Malkov (VINITI, Moscow, 1967), Vol. 2B, p. 336.
[20]J. L. Levine, Phys. Rev. Lett. **15**, 154 (1965).
[21]J. E. Mercereau and L. T. Crane, Phys. Rev. Lett. **9**, 381 (1962).
[22]K. Rose and M. D. Sherrill, Phys. Rev. **145**, 179 (1966).
[23]D. H. Douglass, Jr., Phys. Rev. **132**, 513 (1963).
[24]S. Tolansky, *Multiple Beam Interferometry of Surfaces and Films*, 1st ed. (Clarendon, Oxford, England, 1948).
[25]A. K. Bhatnagar and J. A. Stark, Department of Physics and Astronomy Technical Report No. 606, University of Maryland, 1966 (unpublished).
[26]W. S. Smyth, *Static and Dynamic Electricity* (McGraw-Hill, New York, 1950).
[27]The authors are thankful to Hungerford and Terry Inc., Arlington, Va., for supplying the zeolite free of charge.
[28]M. Tinkham, Phys. Rev. **110**, 26 (1959).
[29]P. G. de Gennes, *Superconductivity of Metals and Alloys* (Benjamin, New York, 1966).
[30]D. H. Douglass, Jr., Phys. Rev. **124**, 735 (1961).
[31]S. Skalski, O. Betbeder-Matibet, and P. R. Weiss, Phys. Rev. **136**, A1500 (1964).
[32]D. H. Douglass Jr., Phys. Rev. Lett. **6**, 346 (1961).
[33]M. Tinkham, Phys. Rev. **129**, 2413 (1963).
[34]A. K. Bhatnagar, Bull. Am. Phys. Soc. **14**, 196 (1969).

PHYSICAL REVIEW B VOLUME 8, NUMBER 3 1 AUGUST 1973

Transition Temperature of d-f-Band Superconductors

J. Appel
I. Institut für Theoretische Physik, der Universität Hamburg, Germany
(Received 20 November 1972)

The theory of Appel and Kohn is used to calculate T_c for a narrow-band superconductor, where the conduction electrons near the Fermi suface have both d and f character. The vertex equations for the symmetrized pair states formed from d and f orbitals are solved in the contact model. The result is used for a parameter study of T_c; one pertinent parameter is the pairing interaction due to phonon exchange between d and f electrons. The experimental situation for La is discussed in terms of the T_c results.

I. INTRODUCTION

We address ourselves to the question: What is the effect on the superconducting transition temperature T_c that is caused by a narrow f band at or near the Fermi surface of a d band? The f band may be "infinitely narrow," corresponding to nonmagnetic and nonconducting f states, or it may have a finite width on account of $f-f$ overlap or covalent $d-f$ admixture. One reason for studying this question is the considerable interest in the mechanism for superconductivity in La and La-Ce alloys.[1-15] Also U has an unusual superconductive behavior, for example, with respect to the pressure dependence of T_c.[6] In metallic La, the electrons at the Fermi surface (FS) have a predominant d character, according to the large d-orbital contribution to the Knight shift and the nuclear spin relaxation in the normal state.[7] The $4f$ levels lie above the Fermi energy, but the distance is not known at present. However, the rare-earth element next to La, namely Ce, in the free atomic state has one bound $4f$ electron, whereas La has none. In the metallic state, Ce has $4f$ levels at or below the Fermi energy. The electrons occupying these levels cause a strong exchange enhancement of the magnetic susceptibility[8] and are responsible for the absence of superconductivity in Ce metal. Therefore, it is reasonable to assume that in La metal the $4f$ levels are close to (but above) the Fermi energy, the distance ϵ_f being of the order of a typical phonon energy $\hbar\omega_0$, where ω_0 is the maximum phonon frequency.

Under the assumption $\epsilon_f \leq \hbar\omega_0$, Kuper, Jensen, and Hamilton[1] have developed a theory of superconductivity in La based on a two-band model. The first band is the conduction band arising from the $5d\,6s^2$ valence electrons. In this band, the BCS